Journal of Materials Chemistry C

PAPER

View Article Online
View Journal | View Issue

Cite this: J. Mater. Chem. C, 2018, 6, 12679

Exploring the effect of the cyclometallating ligand in 2-(pyridine-2-yl)benzo[*d*]thiazole-containing iridium(III) complexes for stable light-emitting electrochemical cells†

Cristina Momblona,‡[a] Cathrin D. Ertl,‡§[b] Antonio Pertegás,[a] José M. Junquera-Hernández,[a] Henk J. Bolink,[a] Edwin C. Constable,[b] Michele Sessolo,*[a] Enrique Ortí*[a] and Catherine E. Housecroft*[b]

Received 18th September 2018,
Accepted 22nd October 2018

DOI: 10.1039/c8tc04727h

rsc.li/materials-c

The preparation and characterization of a series of iridium(III) ionic transition-metal complexes for application in light-emitting electrochemical cells (LECs) are reported. The complexes are of the type $[Ir(C^N)_2(N^N)][PF_6]$ in which C^N is one of the cyclometallating ligands 2-(3-(*tert*-butyl)phenyl)pyridine (tppy), 2-phenylbenzo[*d*]thiazole (pbtz), 1-phenyl-1*H*-pyrazole (ppz) and 1-phenylisoquninoline (piq), and N^N is 2-(pyridine-2-yl)benzo[*d*]thiazole (btzpy). The variation in the C^N ligands allows the HOMO energy level to be tuned, leading to HOMO–LUMO gaps in the range 2.76–3.01 eV and values of $E^{ox}_{1/2}$ of 0.81–1.11 V. In solution, the complexes are orange to deep-red emitters (λ_{max} in the range 600–660 nm), with quantum yields between 2% for $[Ir(tppy)_2(btzpy)][PF_6]$ and 41% for $[Ir(pbtz)_2(btzpy)][PF_6]$. Similar trends for the emission maxima and photoluminescence quantum yields are observed in the solid state. Density functional theory (DFT) calculations support the charge transfer nature of the emission. Very bright electroluminescence was observed for LECs containing $[Ir(pbtz)_2(btzpy)][PF_6]$, although the device was not stable under continuous operation; this is attributed to an unbalanced charge distribution and/or to a fast ionic migration. Significantly, LECs fabricated with $[Ir(tppy)_2(btzpy)][PF_6]$ in the active layer are very stable, produce pure red emission and show no signs of degradation over a period of 5 days of continuous operation.

Introduction

Solid-state lighting (SSL) has emerged as a promising technology taking over from the use of conventional light sources such as incandescent bulbs or fluorescent tubes. Light-emitting electrochemical cells (LECs) are simple and potentially inexpensive SSL devices, where a single molecular material is placed in between two electrodes.[1–5] To date, the most commonly used emissive layer in LECs has been composed of phosphorescent iridium(III) ionic transition-metal complexes (Ir-iTMCs) with general formula $[Ir(C^N)_2(N^N)]^+$, where C^N is a cyclometallating ligand and N^N is an ancillary diimino ligand.[6–9] It is well known that the frontier orbitals in Ir-iTMCs are usually spatially separated. The highest-occupied molecular orbital (HOMO) is localized on the C^N ligands, whereas the lowest-unoccupied molecular orbital (LUMO) resides on the N^N ligand.[10–12] This spatial separation has been used to blue- or red-shift the emission by changing or chemically modifying the ligands around the Ir(III) metal.[13–17]

As the LEC performance is determined by the photophysical and charge-transport properties of the iTMC, its design is crucial for colour tuning as well as for an efficient device operation. Several approaches have been attempted in the chemical modification/functionalization of the archetypal cationic iridium complex $[Ir(ppy)_2(bpy)][PF_6]$ (Hppy = 2-phenylpyridine, bpy = 2,2′-bipyridine) in order to enhance the device performance. For example, the use of bulky groups and spacers has been reported to increase both the device stability and efficiency.[2,18–20] This is due to an enhanced peripheral steric hindrance of the complex, which reduces intermolecular quenching and leads to high PLQY in thin films. However, there are limits in the size of the bulky groups that can be used to decorate the periphery of the complex. Very large substituents would be detrimental for charge transport as a

[a] Instituto de Ciencia Molecular, Universidad de Valencia, C/Catedrático José Beltrán 2, ES-46980 Paterna, Valencia, Spain. E-mail: michele.sessolo@uv.es, enrique.orti@uv.es
[b] Department of Chemistry, University of Basel, BPR 1096, Mattenstrasse 24a, CH-4058 Basel, Switzerland. E-mail: catherine.housecroft@unibas.ch

† Electronic supplementary information (ESI) available: Synthesis and characterization details, theoretical geometrical parameters and spin densities, excited-state lifetime data and electroluminescence data. See DOI: 10.1039/c8tc04727h

‡ These authors contributed equally to this work.

§ Current address: Department of Chemistry, University of British Columbia, 2036 Main Mall, Vancouver, BC V6T 1Z1, Canada.

consequence of the augmented intermolecular separation, increasing the operating voltage of the device. Such groups may also slow down the ion migration within the device, leading to long turn-on times.[19] We reported a breakthrough in the stability of LECs by the use of ligands that favour intramolecular π–π stacking.[21–23] This interaction results in a supramolecularly caged hydrophobic scaffold where the iridium metal centre is more shielded from nucleophilic attacks, which would degrade the emitter and undermine the device operation.

Recently, two families of Ir-iTMC complexes without peripheral bulky substituents have been employed in LECs with high stability and short turn-on times. The first family is based on iTMCs with arylazole-containing ancillary ligands,[24] while the second uses benzothiazole-based ancillary ligands.[25] In the latter case, a series of extremely stable red-emitting LECs based on $[Ir(ppy)_2(btzpy)][PF_6]$ (btzpy = 2-(pyridine-2-yl)benzo[*d*]thiazole) were reported, with a maximum luminance of 200 cd m^{-2} and device lifetime exceeding 6000 hours.[25] In view of the promising optoelectronic properties of these benzothiazole-containing iridium complexes, we have extended the range of compounds incorporating 2-(pyridine-2-yl)benzo[*d*]thiazole (btzpy) as the N^N ligand and investigated the influence of varying the C^N cyclometallated ligands. In this work we report the synthesis, characterization and electroluminescent properties of four new iTMCs with general formula $[Ir(C^N)_2(btzpy)][PF_6]$. The C^N ligands used are 2-(3-(*tert*-butyl)phenyl)pyridine (tppy), 1-phenylisoquinoline (piq), 1-phenyl-1*H*-pyrazole (ppz) and 2-phenylbenzo[*d*]thiazole (pbtz), giving complexes **1**, **2**, **3** and **4**, respectively (Scheme 1). The photo- and electroluminescence confirmed the expected colour variation, ranging from orange to red. Importantly, we obtained very stable devices even when driven with high current density.

Experimental section

Synthesis and compound characterization

Detailed synthetic procedures including characterization data are reported in the ESI.† For reactions performed under an inert atmosphere, dry solvents purchased from Sigma-Aldrich or Acros Organics were used. Solvents used for all other reactions were of reagent grade. Analyses were performed using HPLC grade solvents. Fluka silica gel 60 (0.040–0.063 mm) was used for column chromatography. NMR spectra were recorded on Bruker Avance III-400 (400 MHz) or III-500 (500 MHz) spectrometers and chemical shifts referenced to residual solvent peaks with δ(TMS) = 0 ppm. ESI mass spectrometry was performed using a Bruker Esquire 3000^{plus} instrument and elemental analysis on an Elementar Vario Micro Cube instrument. FT-IR spectra were obtained using a PerkinElmer Spectrum Two UATR instrument. UV-Vis absorption spectra were measured using an Agilent 8453 spectrophotometer and solution emission spectra were recorded on a Shimadzu 5301PC spectrofluorophotometer. Solution and powder photoluminescence quantum yields were recorded on a Hamamatsu absolute PL quantum yield spectrometer C11347 Quantaurus QY. Powder emission spectra as well as solution and powder excited-state lifetime values were obtained using a Hamamatsu Compact Fluorescence lifetime spectrometer C11367 Quantaurus Tau. Electrochemical measurements were carried out using a CH Instruments 900B potentiostat in deaerated CH_2Cl_2 solution, using both glassy carbon and platinum working electrodes, a platinum counter electrode and a silver wire as a pseudo-reference electrode. $TBAPF_6$ (0.1 M) was used as the supporting electrolyte and 3–5 mg of the iridium(III) compound was added to CH_2Cl_2 (10 mL). The scan rate was set as 0.1 mV s^{-1}. Ferrocene was used as the internal reference and was added at the end of each experiment.

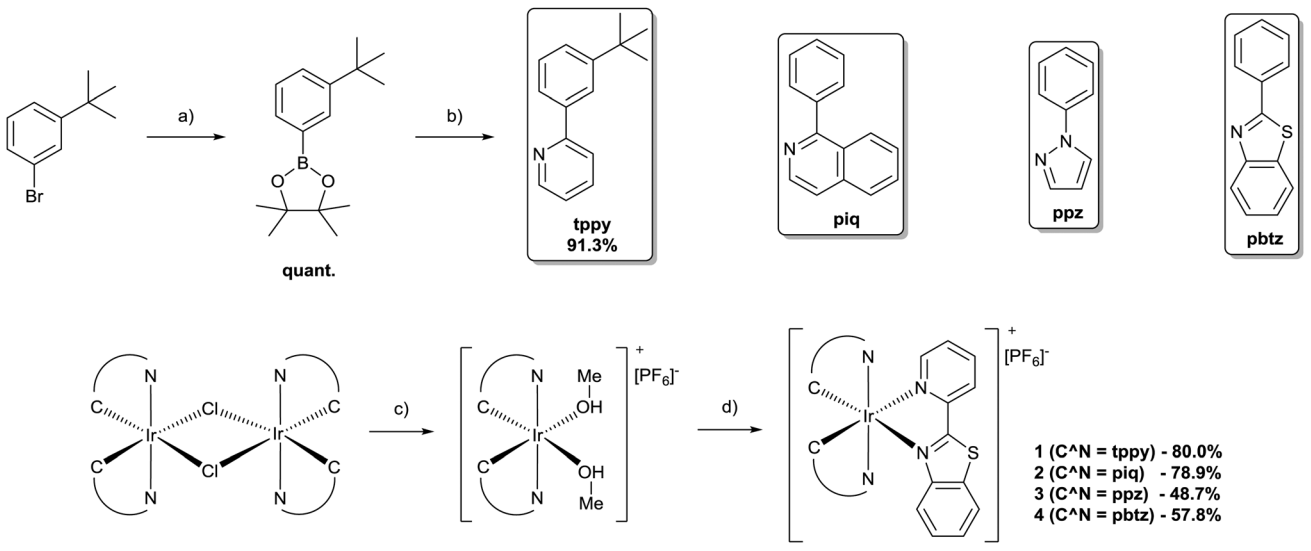

Scheme 1 Synthesis of 2-(3-(*tert*-butyl)phenyl)pyridine (tppy) and iridium complexes **1–4**, and chemical structures of the cyclometallating C^N ligands used. Reaction conditions: (a) bis(pinacolato)diboron, KOAc, $Pd(dppf)_2Cl_2{\cdot}CH_2Cl_2$, THF, MW, 90 °C, 1 h; (b) 2-bromopyridine, Na_2CO_3, $Pd(PPh_3)_2Cl_2$, THF/H_2O 1 : 1, MW, 100 °C, 30 min; (c) $AgPF_6$, MeOH, room temperature, 2.5–4 h; (d) btzpy, MeOH, room temperature, overnight. Reported yields (over two steps) are calculated based on the dimer starting materials.

Photoluminescence characterization

The samples for thin-film photoluminescence (PL) measurements were prepared with the same composition and thickness as the emissive layer used in LECs. Each complex was mixed with the ionic liquid (IL) 1-butyl-3-methylimidazolium hexafluorophosphate ([Bmim][PF_6]) in a molar ratio of 4 : 1. A 100 nm thick film was deposited from a 20 mg mL^{-1} solution of complexes **1–4** in acetonitrile. Prior to deposition, all solutions were filtered with a 0.22 μm pore size filter and spin-coated at 1000 rpm for 30 s in air onto cleaned quartz substrates. The quantum yields and PL spectra in thin films were recorded using a Hamamatsu absolute quantum yield C9920 spectrometer.

Computational details

Density functional calculations (DFT) were performed using the D.01 revision of the Gaussian 09 program package.[26] The Becke's three-parameter B3LYP exchange–correlation functional,[27,28] together with the 6-31G** basis set for C, H, N, and S[29] and the "double-ζ" quality LANL2DZ basis set for the Ir atom,[30] was employed in all the calculations. An effective core potential (ECP) was used to replace the inner core electrons of Ir, accounting for relativistic effects. The geometries of the singlet ground electronic state (S_0) and the lowest-energy triplet state (T_1) were fully optimized for cations $[\mathbf{1}]^+$ to $[\mathbf{4}]^+$. No symmetry restrictions were imposed during the optimization process. The geometries of $[\mathbf{1}]^+$–$[\mathbf{4}]^+$ in the T_1 state were calculated using the spin-unrestricted UB3LYP formulation with spin multiplicity of three. All the calculations were done in the presence of the solvent (CH_2Cl_2). Solvent effects were considered within the self-consistent reaction field (SCRF) theory using the polarized continuum model (PCM) approach.[31–33] The lowest-lying 5 triplet and 10 singlet excited states of all the complexes were computed at the minimum-energy geometry optimized for S_0 using the time-dependent DFT (TD-DFT)[34–36] approach. The phosphorescence emission energies were estimated as the vertical energy difference between the energy of the minimum of T_1 and the single-point energy of S_0 at the T_1 optimized geometry.

Device fabrication

All materials were used as received. Poly(3,4-ethylenedioxythiophene):polystyrene sulfonate (PEDOT:PSS, Clevios P VP Al 4083) was purchased from Heraeus. [Bmim][PF_6] and acetonitrile were purchased from Sigma Aldrich. Photolithography-patterned indium tin oxide (ITO) glass substrates were purchased from Naranjo Substrates (www.naranjosubstrates.com). The substrates were subsequently cleaned with soap, deionized water, and isopropanol in an ultrasonic bath for 5 minutes each, followed by 20 minutes of UV–ozone treatment. Onto the clean ITO substrates, an 80 nm thick film of PEDOT:PSS was spin-coated at 1000 rpm for 1 minute. The PEDOT:PSS dispersion was filtered with a 0.45 μm pore size filter. The layers were dried at 150 °C for 15 minutes. On top of it, a 100 nm thick film of the emissive layer was deposited under the same conditions described above for PL measurements. After deposition, they were transferred to a nitrogen glove box and annealed at 100 °C for 1 hour. Finally, a 70 nm thick aluminium film was thermally deposited under vacuum as the top electrode using a shadow mask.

LEC characterization

LECs were tested by applying pulsed current and by monitoring the voltage and the luminance with a True Colour Sensor (MTCSiCT Sensor, MAZeT GimbH) using a Lifetime Test System (Botest OLT OLED Lifetime-Test System, Botest System GmbH). The pulsed current consisted of a block wave at 1000 Hz frequency with a 50% duty cycle. The current density at the peak of the pulse was 1400 A m^{-2} and the average current density was 700 A m^{-2}. Electroluminescence spectra were recorded using an Avantes fibre optics photo-spectrometer. All devices were tested without encapsulation inside a nitrogen glove-box at room temperature.

Results and discussion

Ligand synthesis

The chemical structures of the cyclometallating C^N ligands used in this series of iridium complexes are shown in Scheme 1, and detailed synthetic procedures are described in the ESI.† The synthesis of tppy has been previously reported,[37] but the following procedure shows a higher yield. 1-Bromo-3-(*tert*-butyl)-benzene was transformed into 2-(3-(*tert*-butyl)phenyl)-4,4,5,5-tetramethyl-1,3,2-dioxaborolane *via* a microwave-assisted Miyaura borylation using bis(pinacolato)diboron and KOAc, catalysed by $Pd(dppf)_2Cl_2{\cdot}CH_2Cl_2$. Suzuki coupling with 2-bromopyridine gave the desired ligand in excellent yields (91.3% over two steps, Scheme 1).

Synthesis of iridium complexes

Chlorido-bridged iridium dimers were prepared according to the standard method[38,39] and characterized by ^{1}H NMR spectroscopy. Cleavage of the iridium dimer with the ancillary ligand in MeOH or CH_2Cl_2/MeOH is the typical procedure for the synthesis of iridium complexes of the type $[Ir(C^N)_2(N^N)]^+$.[40–42] However, by using this protocol, traces of chloride counterions may still be present in the final product, despite using a large excess of hexafluorophosphate salt for ion metathesis. We have shown that even small amounts of chloride impurities can significantly decrease the stability of a LEC.[43] Therefore, complexes **1–4** were synthesized according to a two-step procedure *via* a solvento intermediate, formed by the reaction of the iridium dimer with $AgPF_6$ in MeOH (Scheme 1). Exchange of the bound solvent molecules by the ancillary ligand subsequently occurs at room temperature in MeOH solution. This method has previously been successfully implemented in the synthesis of a series of orange emitters, leading to exceptional device stabilities.[43] As shown in Scheme 1, iridium complexes **1–4** were obtained in moderate to high yields (over two steps) starting from the appropriate dimer and the ancillary ligand btzpy, and were fully characterized by 1D and 2D NMR spectroscopies, ESI mass spectrometry, elemental analysis and IR spectroscopy (see the ESI† for details).

Theoretical calculations: geometry and molecular orbitals

The geometries of the complexes in their ground electronic state S_0 were theoretically optimized without imposing any symmetry restriction using DFT calculations at the B3LYP/(6-31G**+LANL2DZ) level and including solvent effects (CH_2Cl_2). The optimized geometries reproduce the near-octahedral coordination of the Ir metal usually found in this series of iridium complexes,[44,45] and those previously reported for other complexes including btzpy as the ancillary ligand.[25] The minimum-energy geometries computed for the cations of complexes **1–4** are depicted in Fig. 1, and the selected geometrical parameters are listed in Table S1 (ESI†). As for the reference $[Ir(ppy)_2(btzpy)]^+$ complex,[25] and due to the absence of pendant groups that give rise to intramolecular stacking, both the cyclometallating and the ancillary ligands in all the complexes are predicted to be mainly planar. Only in the piq ligands, where the additional phenyl ring causes intra-ligand H···H contacts that break the planarity, the inter-ring dihedral angle rises to ~17° (see Table S1, ESI†).

The energies calculated for the HOMO and LUMO of complexes **1–4** are displayed in Fig. 2. The topology of the frontier molecular orbitals remains almost unchanged along the series, and only the HOMO and LUMO of complex **1** are depicted. As it is usually found for ionic cyclometallated iridium complexes,[45,46] including those previously studied with a btzpy ancillary ligand,[25] the HOMO appears mainly centred on the metal and the phenyl rings of the C^N ligands, whereas the LUMO is almost fully located on the N^N ligand. As the LUMO resides on a molecular region that remains structurally unchanged along the series, its energy remains almost constant for all the complexes, and is very close to that of $[Ir(ppy)_2(btzpy)]^+$ (−2.98 eV). In contrast, the energy of the HOMO changes with the nature of the cyclometallating ligand. The electron-donating nature of the *tert*-butyl group induces a destabilization of the HOMO of complex **1** (−5.72 eV), which is computed 0.14 eV higher in energy than the HOMO of $[Ir(ppy)_2(btzpy)]^+$ (−5.86 eV). The 1-phenylisoquinoline ligand induces a smaller destabilization of the HOMO in **2** (−5.82 eV). In complexes **3** and **4**, the substitution of the pyridine ring of the C^N ligands by a more electron-deficient heterocycle produces a stabilization of the HOMO,[47] which now appears at −5.95 and −6.02 eV, respectively. As a consequence, the HOMO–LUMO energy gap increases along the series **1–4** from 2.76 to 3.01 eV, with complexes **1** and **2** having smaller, and complexes **3** and **4** greater HOMO–LUMO gaps, than that of $[Ir(ppy)_2(btzpy)]^+$ (2.88 eV). Therefore, if the emitting triplet state results from the HOMO → LUMO excitation, complexes **1** and **2** are expected to emit at longer wavelengths as compared to complexes **3** and **4**.

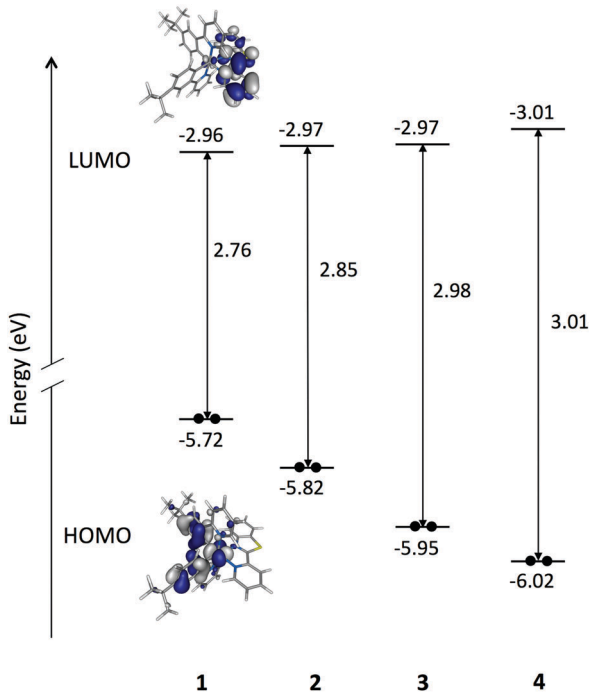

Fig. 2 Energy diagram showing the energies calculated for the HOMO and LUMO of complexes **1–4**. The HOMO–LUMO energy gap is also quoted. Isovalue contour plots (±0.03 a.u.) are drawn for the HOMO and LUMO of complex **1** (C^N = tppy). The topology of the frontier MOs of the other complexes is almost identical and is omitted for simplicity.

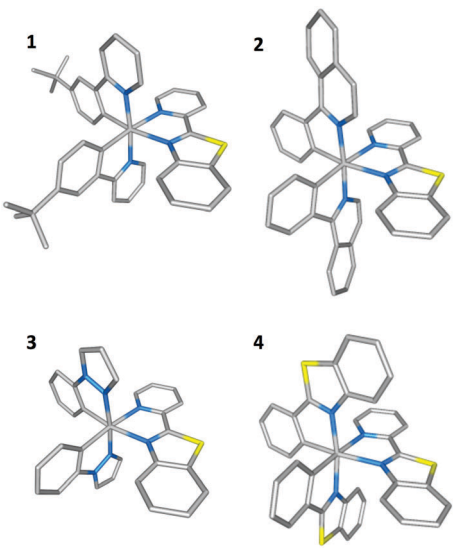

Fig. 1 B3LYP/(6-31G**+LANL2DZ)-optimized geometries for the ground state S_0 of complexes **1–4**. Hydrogen atoms are omitted for simplicity.

Electrochemical properties

The electrochemical data of complexes **1–4**, obtained from cyclic voltammetry measurements in CH_2Cl_2 solution, are summarized in Table 1. The reduction potentials lie in a close range (−1.52 to −1.57 V, Fig. 3), in agreement with the energies computed for the LUMO that also lie in the 0.05 eV range as a consequence of the localization of the LUMO on the ancillary btzpy ligand (Fig. 2). Since the HOMO is localized mainly on the iridium centre and the phenyl ring of the cyclometallating ligand, the oxidation potential is sensitive to changes in the C^N ligand and follows the trends of the HOMO energies predicted by DFT calculations. Complexes **1** and **2**, the HOMOs of which are computed at higher energies (Fig. 2), are more readily oxidized than complexes **3** and **4** (Table 1). This is in

Table 1 Electrochemical data of complexes **1–4** referenced to Fc/Fc^{+} [a]

Complex	$E^{ox}_{1/2}$ [V] ($E_{pa} - E_{pc}$ [mV])	$E^{red}_{1/2}$ [V] ($E_{pc} - E_{pa}$ [mV])	$\Delta E_{1/2}$ [V]
1	$+0.81^{qr}$ (113)	−1.56 (100)	2.37
2	$+0.92^{qr}$ (109)	−1.56 (98)	2.48
3	$+1.02^{qr}$ (121)	-1.57^{qr} (103)	2.59
4	$+1.11^{qr}$ (113)	−1.52 (91)	2.63

[a] Determined by cyclic voltammetry in deaerated CH_2Cl_2 solution with Pt working and counter electrodes and an Ag pseudo-reference electrode, 0.1 M $TBAPF_6$ as the electrolyte and a scan rate of 0.1 mV s^{-1}. qr = quasi-reversible.

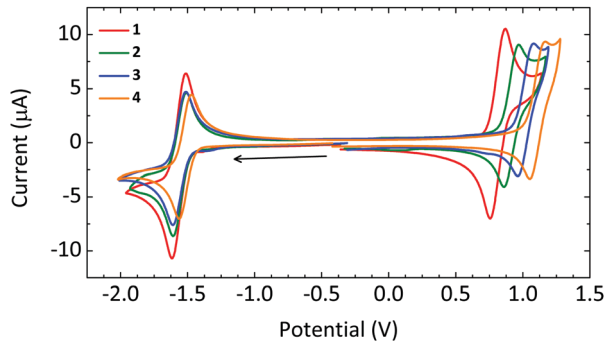

Fig. 3 Cyclic voltammogram traces of complexes **1–4**, measured in CH_2Cl_2 solution and referenced to Fc/Fc^{+}. The arrow indicates the initial scanning direction.

good agreement with the calculated stabilization of the HOMO on going from **1** to **4** (Fig. 2). The oxidation potentials measured for **1–4** span a range below and above that measured for $[Ir(ppy)_2(btzpy)][PF_6]$ (+0.94 V)[25] in good agreement with the theoretical predictions.

Photophysical properties

The UV-Vis absorption spectra of **1–4** in CH_2Cl_2 solution are shown in Fig. 4. Intense absorption bands in the UV with maxima between 253 and 324 nm are seen for all complexes and are attributed to spin-allowed $\pi \rightarrow \pi^*$ transitions of the ligands. Higher wavelength bands in the range 350–450 nm arise from spin-allowed metal-to-ligand (^{1}MLCT) and ligand-to-ligand charge transfer (^{1}LLCT) transitions. Time-dependent DFT (TD-DFT) calculations of the excited singlet states (S_n) confirm this assignment. Complexes **2** and **4** present medium intense maxima above 430 nm due to $S_0 \rightarrow S_n$ low energy $\pi \rightarrow \pi^*$ transitions associated with the more conjugated piq and pbtz ligands, respectively. In addition, low intensity tails above 450 nm are observed (Fig. 4), which are attributed to spin-forbidden ^{3}MLCT, ^{3}LLCT and ligand-centred (^{3}LC) excitations.[45] TD-DFT calculations of the first triplet excited states (T_n) show that in all cases the T_1 state corresponds to the HOMO → LUMO excitation, which implies an electron transfer from the $Ir(C^N)_2$ environment to the N^N ligand (see Fig. 2), and therefore implies a mixed ^{3}MLCT/^{3}LLCT nature.

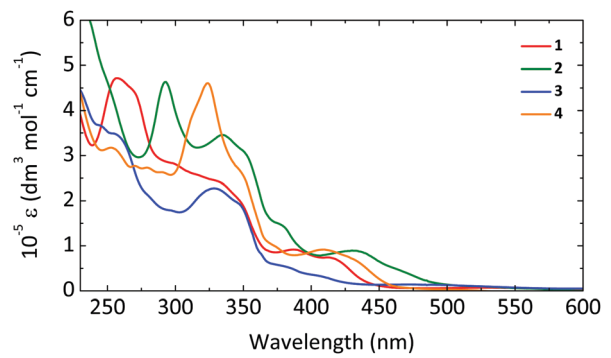

Fig. 4 UV-Vis absorption spectra in CH_2Cl_2 solution (10^{-5} M) of complexes **1–4**.

The absorption spectra of complexes **1** and **3** are similar to that previously reported for $[Ir(ppy)_2(btzpy)][PF_6]$,[25] whereas complexes **2** and **4** show distinct absorption profiles (Fig. 4). Characteristic peaks at 293 (ε = 46 000 dm^3 mol^{-1} cm^{-1}) and 433 nm (ε = 8900 dm^3 mol^{-1} cm^{-1}) are observed in the absorption spectrum of complex **2** which arise due to the presence of the 1-phenylisoquinoline (piq) cyclometallating ligand. These maxima are also observed for $[Ir(piq)_2(bpy)][PF_6]$ at 290/291 and 439/440 nm (in CH_2Cl_2) with similar extinction coefficients, as described in the literature.[48–50] The distinctive absorption band at 324 nm (ε = 46 000 dm^3 mol^{-1} cm^{-1}) for complex **4** is not present in the other compounds and must therefore be a characteristic of the pbtz cyclometallating ligand. Comparison with literature data of $[Ir(pbtz)_2(bpy)]^+$ shows the presence of an absorption band with two maxima in the same region (310–325 nm) in CH_2Cl_2,[51] CH_3CN,[51] MeOH[52] and THF[53] solutions. TD-DFT calculations support these assignments. For all the four complexes, the $S_0 \rightarrow S_1$ transition associated with the HOMO → LUMO excitation has a negligible oscillator strength ($f < 0.0005$), and the absorption bands observed correspond to transitions to higher excited singlets (S_3 and S_4). For complexes **2** and **4**, these transitions imply the pbtz and piq ligands, respectively, and are calculated at higher wavelengths (≈445 and 420 nm) than for complexes **1** and **3** (400–410 nm). This justifies the red shift observed for **2** and **4** compared with **1** and **3**, which is not expected on the basis of CV values obtained for the electrochemical gap (Table 1).

The PL spectra for the series of compounds were recorded in solution, powder and thin-films. The photophysical parameters are summarized in Table 2. The PL maxima in dichloromethane solutions (10^{-5} M, Fig. 5) are located in the orange to deep-red spectral region, between 600 and 660 nm. Compared to $[Ir(ppy)_2(btzpy)]^+$,[25] functionalization of the cyclometallating ligand with a *tert*-butyl group (complex **1**) red-shifts the emission by 16 nm, whereas substitution of ppy by piq (complex **2**) exerts a negligible influence on the luminescence maximum. As for complexes **3** and **4**, both ppz and pbtz cyclometallating ligands stabilize the HOMO and increase the HOMO–LUMO gap (Fig. 2). Both complexes are therefore orange emitters, with blue-shifted λ^{max}_{em} values of 607 and 600 nm, respectively. These observations agree with the trends observed in the electrochemically measured energy gaps (Table 1). The solution photoluminescence quantum yields and the excited-state lifetimes differ considerably between the

Table 2 Photophysical properties of complexes **1–4**

	CH_2Cl_2 solution			Powder			Film	
Complex	$\lambda_{em}^{max\,a}$ [nm]	$\tau^{b,c}$ [ns]	PLQY^{a,d} [%]	$\lambda_{em}^{max\,b}$ [nm]	$\tau^{b,e}$ [ns]	PLQY^{a} [%]	$\lambda_{em}^{max\,f}$ [nm]	PLQY^{f} [%]
1	660	55	2	648	328	10	666	5
2	642	380^{e}	9	642	142	2	659	3
3	607	459	16	612	337	11	629	12
4	600	1200	41	614	730	33	625	29

^{a} λ_{exc} = 268 nm for complex **1**, 293 nm for **2**, 261 nm for **3** and 326 nm for **4**. ^{b} λ_{exc} = 280 nm for complexes **1–3** and 340 nm for **4**. ^{c} Measured in deaerated solution under an atmosphere of argon. ^{d} Measured in deaerated solution. ^{e} τ_{ave} (biexponential fits were used for the excited-state lifetime determination). ^{f} λ_{exc} = 320 nm.

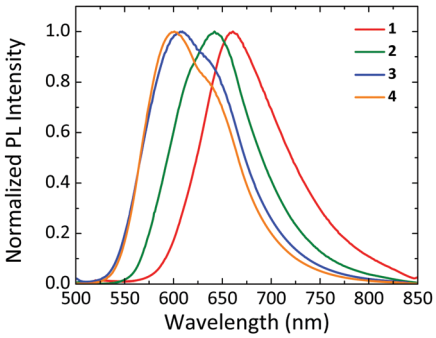

Fig. 5 Emission spectra in CH_2Cl_2 solution (1.0×10^{-5} mol dm^{-3}). λ_{exc} = 430 nm for complex **3**; λ_{exc} = 435 nm for **1**; λ_{exc} = 437 nm for **2** and **4**.

four complexes, with PLQYs ranging from 2% to 41% and lifetimes between 55 ns and 1.2 μs (see Table 2).

Complexes **1–4** show broad, mostly unstructured emission profiles (Fig. 5), indicating a large charge transfer characteristic of the emissive state. This is in good agreement with the ^{3}MLCT/^{3}LLCT (HOMO → LUMO) nature of the emitting T_1 state as predicted by TD-DFT calculations. However, compounds **3** and **4** show some vibrational structures in the emission bands, suggesting a ^{3}LC contribution to the emissive state. To investigate this possibility, the nature of the T_1 triplet was further studied by fully relaxing the molecular geometry of this state using the UDFT approach. It should be recalled that TD-DFT calculations are performed at the optimized geometry of the S_0 ground state (Franck–Condon region), and the order of the states could change upon relaxation. Fig. S1 (ESI†) displays the unpaired-electron spin-density distributions computed for the fully-optimized T_1 triplet of complexes **1–4**. For all the complexes, the unpaired electrons reside over the Ir(C^N)$_2$ environment and the N^N ligand and reproduce the topology of the HOMO → LUMO excitation, thus confirming the charge transfer ^{3}MLCT/^{3}LLCT nature of the emitting state. However, the spin density of complexes **3** and **4** is more concentrated over the N^N ligand which shows a smaller contribution from the metal ($\sim 0.42e$) compared to complexes **1** and **2** ($\sim 0.48e$), thus justifying the appearance of some vibrational structures. The emission energies calculated from the UDFT optimized geometry of T_1 (**1**: 739 nm > **2**: 708 nm > [Ir(ppy)$_2$(btzpy)]$^+$: 691 nm > **3**: 663 nm ≈ **4**: 668 nm), although shifted to the red, reproduce the main trends observed experimentally (Table 2). Complexes **1** and **2** emit more to the red compared to [Ir(ppy)$_2$(btzpy)]$^+$, and complexes **3** and **4** more to the blue region.

The PL spectra of powder samples are shown in Fig. 6a. Whereas no shift of the emission maximum is observed for complex **2** on going from solution to the solid state, we observed a blue-shift (12 nm) for complex **1** and a small red-shift for both complexes **3** and **4** (5 and 14 nm, respectively). As in solution, the solid-state PLQYs of the complexes vary considerably and range from 2% for compound **2** to 33% for complex **4**. The film and solid-state PLQY values follow the same trends as expected. Biexponential fits were used for the decay curves of powder samples of all complexes (Table S2, ESI†). The average lifetimes lie between 142 and 730 ns, with complex **4** exhibiting not only the highest quantum yield, but also the longest lifetime.

Light-emitting electrochemical cells (LECs)

The electroluminescent properties of complexes **1–4** were investigated by preparing LECs using a two-layer architecture, as described

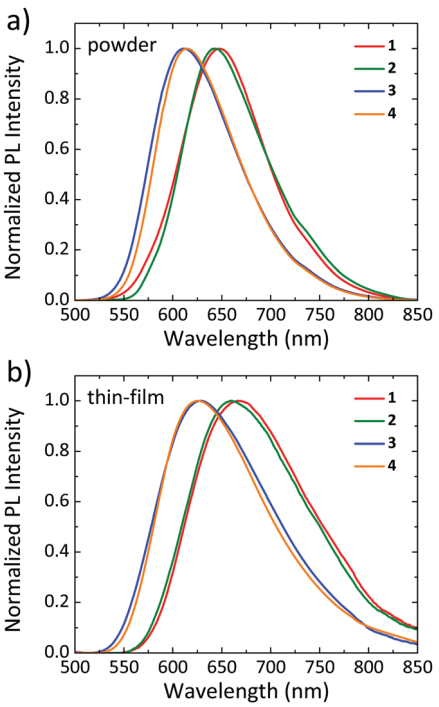

Fig. 6 Solid-state emission spectra of complexes **1–4** in (a) powder (λ_{exc} = 280 nm) and (b) thin-film (λ_{exc} = 320 nm).

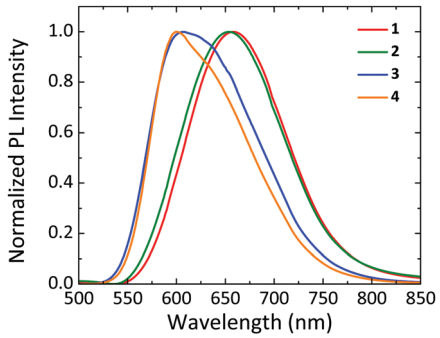

Fig. 7 Normalized electroluminescence spectra of LECs **1–4**.

in the Experimental section. In the following discussion, LECs fabricated using complexes **1–4** will be referred to as LECs **1–4**. As previously mentioned, the emissive layer consists of a mixture of the complex and the IL [Bmim][PF_6] in a molar ratio of 4 : 1. The addition of IL reduces the device turn-on time (t_{on}), defined in this work as the time to reach a luminance of 50 cd m^{-2}.[54] LECs were operated by applying a pulsed-current with an average current density of 700 A m^{-2}, which consists of a block wave at 1000 Hz frequency with a duty cycle of 50%. These driving conditions were used as similar compounds have been found to sustain such high current density with no discernible degradation.[25]

The electroluminescence (EL) spectra for all complexes are displayed in Fig. 7, and the corresponding EL emission maxima and the CIE 1931 colour coordinates are listed in Table 3. LECs **1** and **2** show pure red electroluminescence, with emission maxima centred at 658 and 654 nm and CIE coordinates of (0.65, 0.34) and (0.63, 0.35), respectively. LECs **3** and **4** resulted in orange light emission with main maxima at 607 (LEC **3**) and 600 nm (LEC **4**), and the same CIE coordinates (0.60, 0.40). The EL spectra are similar to the thin-film PL spectra, with a small blue-shift of 8 and 5 nm for the red-emitting devices LEC **1** and LEC **2**, respectively, and a blue-shift of 22 and 25 nm for the orange-emitting devices LEC **3** and LEC **4**, respectively.

The evolution of the luminance and the average voltage was continuously monitored for 120 hours (5 days, Fig. 8) in order to extract the characteristic device parameters, reported in Table 3. LEC **4** presents the largest t_{on} of the series with 1925 s (32 min) to reach 50 cd m^{-2}, while LECs **1–3** exhibit short turn-on times (t_{on}) with values between 13 and 40 s. This feature hints towards a very different ionic redistribution and/or charge injection and transport for LEC **4** within the series.

The orange-emitting LECs **3** and **4** were found to be brighter compared to the red-emitting LECs **1** and **2**. In particular, LEC **4** delivers a maximum luminance (Lum_{max}) of 1049 cd m^{-2}, much higher than LEC **3** (320 cd m^{-2}), LEC **1** (203 cd m^{-2}) and LEC **2** (85 cd m^{-2}). Notably, the maximum luminance in LEC **4** is even higher compared to previously reported ppy-containing compounds.[26] LEC **4** also presents the highest external quantum efficiency (EQE) of the series with 0.91%, whereas an intermediate value of 0.30% was obtained for LEC **3**. The higher luminance obtained for LEC **1** also results in an improved EQE (0.45%) as compared to LEC **2** (0.16%). The general EQE trend agrees with that observed for the PLQY measured in thin-films (Table 2), where **4** (28.7%) > **3** (11.5%) > **1** (5.1%) > **2** (3.3%). Considering the relationship between the EQE and the PLQY, we can investigate the origin of the losses associated with the device efficiency. The EQE can be expressed as follows:

$$EQE = \eta_0 \gamma \zeta_S PLQY$$

where η_0 is the outcoupling efficiency, γ is the electron–hole balance and ζ_S is the exciton generation efficiency. For phosphorescent emitters, the exciton generation efficiency can be considered as unity since all electron–hole pairs can in principle be harvested as emitting triplet excitons. If we deliberately neglect the charge carrier balance ($\gamma = 1$) and reasonably assume $\eta_0 = 0.2$, then we can calculate the theoretical maximum EQE (EQE_{theor}, Table 3) for the device series. By comparing these values with the measured maximum EQEs, we can quantify the losses for each device as $EQE_{losses} = EQE/EQE_{theor}$% (Table 3). We found that orange-emitting LECs **3–4** exhibit larger losses in device efficiency (88 and 84%, respectively), in spite of being the brightest devices obtained. On the other hand, the red-emitting devices exhibit lower losses, in particular LEC **1** where 55% of the charges are non-radiatively lost during the device operation. Such losses are associated with the previously neglected charge-carrier balance, indicating that carrier injection or transport (most likely a combination of both) within the diode are hindered when moving from complex **1** to **4**. At short time scale, when ions have not yet redistributed, the charge injection efficiency is proportional to the potential difference between the electrode work function and the corresponding molecular orbital. As the LUMO energy is essentially unvaried for the compounds presented here, the variation of the HOMO energy from complex **1** to complex **4** (increasing approximately 0.1 eV for each complex within the series, Fig. 2) leads to hindered

Table 3 Performance parameters and electroluminescence data obtained for LECs **1–4** operating under a pulsed-current driving of 700 A m^{-2} (1000 Hz, 50% duty cycle, block wave)

LEC	Lum_{max}[a] [cd m^{-2}]	t_{on}[b] [s]	$t_{1/2}$[c] [h]	EQE_{max}[d] [%]	EQE_{theor}[d] [%]	EQE_{losses} [%]	λ_{em}^{max} EL [nm]	CIE[e]
1	203	13	[g]	0.45	1.0	55	658	0.65, 0.34
2	85	18	220[f]	0.16	0.6	73	654	0.63, 0.35
3	320	38	175[f]	0.30	2.4	88	607	0.60, 0.40
4	1049	1925	26	0.91	5.8	84	600	0.60, 0.40

[a] Maximum luminance. [b] Time to reach 50 cd m^{-2} luminance. [c] Time to decay to half of the maximum luminance. [d] Maximum external quantum efficiency. [e] The CIE 1931 colour coordinates. [f] Extrapolated values. [g] No signs of degradation after 5 days of continuous operation.

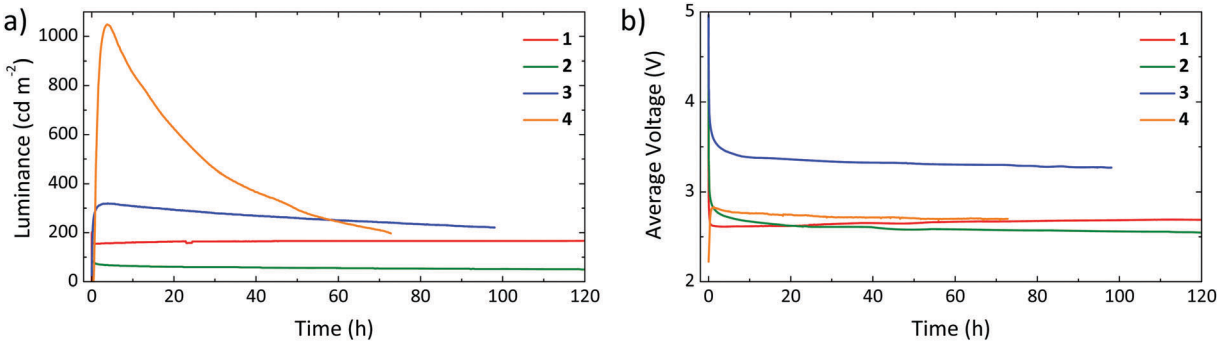

Fig. 8 (a) Luminance and (b) average voltage for LECs **1–4** measured using a pulsed current driving (average current density 700 A m^{-2}, 1000 Hz, 50% duty cycle, block wave).

hole injection from the anode into the active layer, partially explaining the augmented electronic losses. Additionally, the chemical nature and steric hindrance of the cyclometallating ligands vary substantially, resulting in an alteration of the charge transport and balance within the devices. The charge balance within the device should be also reflected in the device lifetime ($t_{1/2}$), defined as the time to decay to one-half of the maximum luminance. In agreement with this hypothesis, LEC **1** actually shows no luminance decay during 5 days of continuous operation (Fig. 8a). The $t_{1/2}$ obtained for LECs **2** and **3** were estimated by extrapolation to be about 220 and 175 hours, respectively (Fig. S2, ESI†). On a side note, LEC **3** showed a larger voltage (approximately 3.3 V after stabilization, Fig. 8b) as compared to the other devices (2.6–2.7 V), indicating a lower conductivity of the complex in the solid state. The brightest device obtained, LEC **4**, showed a very short lifetime of only 26 hours, pointing to an unbalanced charge distribution or to a faster ionic migration under an applied field. The very stable voltage profile (Fig. 8b) also supports the latter hypothesis.

Conclusions

In conclusion, we have synthesized a new family of iTMCs for application in LECs. The variation in the cyclometallating ligand in four $[Ir(C^N)_2(btzpy)][PF_6]$ complexes allows the tuning of the HOMO energy, and thereby the oxidation potential (0.81–1.11 V), and the HOMO–LUMO gap (2.76–3.01 eV). In solution, the complexes present photoluminescence maxima in the orange to deep-red spectral region, between 600 and 660 nm, with significantly different quantum yields ranging from 2% for $[Ir(tppy)_2(btzpy)][PF_6]$ where tppy = 2-(3-(*tert*-butyl)phenyl)pyridine, to 41% for $[Ir(pbtz)_2(btzpy)][PF_6]$ where pbtz = 2-phenylbenzo[*d*]-thiazole. Similar trends for the emission maxima and PLQYs are found in the solid state. DFT calculations support the charge transfer nature of the emission. We obtained very bright electroluminescence for $[Ir(pbtz)_2(btzpy)][PF_6]$. However, the device was not stable under continuous operation, most likely due to an unbalanced charge distribution and/or to a fast ionic migration. Importantly, we have fabricated very stable LECs when using $[Ir(tppy)_2(btzpy)][PF_6]$ in the emissive layer. This complex leads to pure red emission and show no signs of degradation during 5 days of continuous operation, challenging the most stable LECs demonstrated up to now.

Conflicts of interest

There are no conflicts to declare.

Acknowledgements

This work was supported by the Spanish Ministry of Economy and Competitiveness (MINECO) (MAT2014-55200, CTQ2015-71154-P, and Unidad de Excelencia María de Maeztu MDM-2015-0538), the Generalitat Valenciana (PROMETEO/2016/135), European Feder Funds (CTQ2015-71154-P), the Swiss National Science Foundation (Grant numbers 200020_144500 and 200020_162631) and the University of Basel. C. M. and M. S. thank the MINECO for their predoctoral and RyC contract, respectively.

Notes and references

1 Q. Pei, G. Yu, C. Zhang, Y. Yang and A. J. Heeger, *Science*, 1995, **269**, 1086–1088.
2 J. D. Slinker, A. A. Gorodetsky, M. S. Lowry, J. Wang, S. Parker, R. Rohl, S. Bernhard and G. G. Malliaras, *J. Am. Chem. Soc.*, 2004, **126**, 2763–2767.
3 J. D. Slinker, J. Rivnay, J. S. Moskowitz, J. B. Parker, S. Bernhard, H. D. Abruna and G. G. Malliaras, *J. Mater. Chem.*, 2007, **17**, 2976–2988.
4 Q. Sun, Y. Li and Q. Pei, *J. Disp. Technol.*, 2007, **3**, 211–224.
5 E. Fresta and R. D. Costa, *J. Mater. Chem. C*, 2017, **5**, 5643–5675.
6 K. P. S. Zanoni, R. L. Coppo, R. C. Amaral and N. Y. Murakami Iha, *Dalton Trans.*, 2015, **44**, 14559–14573.
7 A. F. Henwood and E. Zysman-Colman, *Top. Curr. Chem.*, 2016, **374**, 36.
8 D. Ma, T. Tsuboi, Y. Qiu and L. Duan, *Adv. Mater.*, 2017, **29**, 1603253.
9 C. E. Housecroft and E. C. Constable, *Coord. Chem. Rev.*, 2017, **350**, 155–177.

10 M. S. Lowry, W. R. Hudson, R. A. Pascal and S. Bernhard, *J. Am. Chem. Soc.*, 2004, **126**, 14129–14135.
11 C. Dragonetti, L. Falciola, P. Mussini, S. Righetto, D. Roberto, R. Ugo, A. Valore, F. De Angelis, S. Fantacci, A. Sgamellotti, M. Ramon and M. Muccini, *Inorg. Chem.*, 2007, **46**, 8533–8547.
12 H. J. Bolink, E. Coronado, R. D. Costa, N. Lardiés and E. Ortí, *Inorg. Chem.*, 2008, **47**, 9149–9151.
13 C. D. Ertl, L. Gil-Escrig, J. Cerdá, A. Pertegás, H. J. Bolink, J. M. Junquera-Hernández, A. Prescimone, M. Neuburger, E. C. Constable, E. Ortí and C. E. Housecroft, *Dalton Trans.*, 2016, **45**, 11668–11681.
14 M. Mydlak, C. Bizzarri, D. Hartmann, W. Sarfert, G. Schmid and L. De Cola, *Adv. Funct. Mater.*, 2010, **20**, 1812–1820.
15 C. Fan, Y. Li, C. Yang, H. Wu, J. Qin and Y. Cao, *Chem. Mater.*, 2012, **24**, 4581–4587.
16 C. D. Ertl, J. Cerdá, J. M. Junquera-Hernández, A. Pertegás, H. J. Bolink, E. C. Constable, M. Neuburger, E. Ortí and C. E. Housecroft, *RSC Adv.*, 2015, **5**, 42815–42827.
17 D. L. Davies, M. P. Lowe, K. S. Ryder, K. Singh and S. Singh, *Dalton Trans.*, 2011, **40**, 1028–1030.
18 H. C. Su, F. C. Fang, T. Y. Hwu, H. H. Hsieh, H. F. Chen, G. H. Lee, S. M. Peng, K. T. Wong and C. C. Wu, *Adv. Funct. Mater.*, 2007, **17**, 1019–1027.
19 C. Rothe, C.-J. Chiang, V. Jankus, K. Abdullah, X. Zeng, R. Jitchati, A. S. Batsanov, M. R. Bryce and A. P. Monkman, *Adv. Funct. Mater.*, 2009, **19**, 2038–2044.
20 D. Tordera, A. Pertegás, N. M. Shavaleev, R. Scopelliti, E. Ortí, H. J. Bolink, E. Baranoff, M. Grätzel and M. K. Nazeeruddin, *J. Mater. Chem.*, 2012, **22**, 19264–19268; C. Hierlinger, E. Trzop, L. Toupet, J. Ávila, M.-G. La-Placa, H. J. Bolink, V. Guerchais and E. Zysman-Colman, *J. Mater. Chem.*, 2018, **6**, 6385–6397.
21 R. D. Costa, E. Ortí, H. J. Bolink, S. Graber, C. E. Housecroft and E. C. Constable, *J. Am. Chem. Soc.*, 2010, **132**, 5978–5980.
22 H. J. Bolink, E. Coronado, R. D. Costa, E. Ortí, M. Sessolo, S. Graber, K. Doyle, M. Neuburger, C. E. Housecroft and E. C. Constable, *Adv. Mater.*, 2008, **20**, 3910–3913.
23 S. Graber, K. Doyle, M. Neuburger, C. E. Housecroft, E. C. Constable, R. D. Costa, E. Ortí, D. Repetto and H. J. Bolink, *J. Am. Chem. Soc.*, 2008, **130**, 14944–14945.
24 M. Martínez-Alonso, J. Cerdá, C. Momblona, A. Pertegás, J. M. Junquera-Hernández, A. Heras, A. M. Rodríguez, G. Espino, H. Bolink and E. Ortí, *Inorg. Chem.*, 2017, **56**, 10298–10310.
25 C. D. Ertl, C. Momblona, A. Pertegás, J. M. Junquera-Hernández, M.-G. La-Placa, A. Prescimone, E. Ortí, C. E. Housecroft, E. C. Constable and H. J. Bolink, *J. Am. Chem. Soc.*, 2017, **139**, 3237–3248.
26 M. J. Frisch, G. W. Trucks, H. B. Schlegel, G. E. Scuseria, M. A. Robb, J. R. Cheeseman, G. Scalmani, V. Barone, B. Mennucci, G. A. Petersson, H. Nakatsuji, M. Caricato, X. Li, H. P. Hratchian, A. F. Izmaylov, J. Bloino, G. Zheng, J. L. Sonnenberg, M. Hada, M. Ehara, K. Toyota, R. Fukuda, J. Hasegawa, M. Ishida, T. Nakajima, Y. Honda, O. Kitao, H. Nakai, T. Vreven, J. A. Montgomery Jr., J. E. Peralta, F. Ogliaro, M. J. Bearpark, J. Heyd, E. N. Brothers, K. N. Kudin, V. N. Staroverov, R. Kobayashi, J. Normand, K. Raghavachari, A. P. Rendell, J. C. Burant, S. S. Iyengar, J. Tomasi, M. Cossi, N. Rega, N. J. Millam, M. Klene, J. E. Knox, J. B. Cross, V. Bakken, C. Adamo, J. Jaramillo, R. Gomperts, R. E. Stratmann, O. Yazyev, A. J. Austin, R. Cammi, C. Pomelli, J. W. Ochterski, R. L. Martin, K. Morokuma, V. G. Zakrzewski, G. A. Voth, P. Salvador, J. J. Dannenberg, S. Dapprich, A. D. Daniels, Ö. Farkas, J. B. Foresman, J. V. Ortiz, J. Cioslowski and D. J. Fox, *Gaussian 09, Revision D.01*, Gaussian, Inc., Wallingford CT, 2009.
27 C. Lee, W. Yang and R. G. Parr, *Phys. Rev. B: Condens. Matter Mater. Phys.*, 1988, **37**, 785–789.
28 A. D. Becke, *J. Chem. Phys.*, 1993, **98**, 5648–5652.
29 M. M. Francl, W. J. Pietro, W. J. Hehre, J. S. Binkley, M. S. Gordon, D. J. DeFrees and J. A. Pople, *J. Chem. Phys.*, 1982, **77**, 3654–3665.
30 P. J. Hay and W. R. Wadt, *J. Chem. Phys.*, 1985, **82**, 299–310.
31 J. Tomasi and M. Persico, *Chem. Rev.*, 1994, **94**, 2027–2094.
32 C. S. Cramer and D. G. Truhlar, *Solvent Effects and Chemical Reactivity*, *Kluwer*, 1996, pp. 1–80.
33 J. Tomasi, B. Mennucci and R. Cammi, *Chem. Rev.*, 2005, **105**, 2999–3094.
34 M. E. Casida, C. Jamorski, K. C. Casida and D. R. Salahub, *J. Chem. Phys.*, 1998, **108**, 4439–4449.
35 C. Jamorski, M. E. Casida and D. R. Salahub, *J. Chem. Phys.*, 1996, **104**, 5134–5147.
36 M. Petersilka, U. J. Gossmann and E. K. U. Gross, *Phys. Rev. Lett.*, 1996, **76**, 1212–1215.
37 A. Singh, K. Teegardin, M. Kelly, K. S. Prasad, S. Krishnan and J. D. Weaver, *J. Organomet. Chem.*, 2015, **776**, 51–59.
38 S. Sprouse, K. A. King, P. J. Spellane and R. J. Watts, *J. Am. Chem. Soc.*, 1984, **106**, 6647–6653.
39 F. O. Garces, K. A. King and R. J. Watts, *Inorg. Chem.*, 1988, **27**, 3464–3471.
40 D. Tordera, A. M. Bünzli, A. Pertegás, J. M. Junquera-Hernández, E. C. Constable, J. A. Zampese, C. E. Housecroft, E. Ortí and H. J. Bolink, *Chem. – Eur. J.*, 2013, **19**, 8597–8609.
41 F. Neve, A. Crispini, S. Campagna and S. Serroni, *Inorg. Chem.*, 1999, **38**, 2250–2258.
42 R. D. Costa, E. Ortí, D. Tordera, A. Pertegás, H. J. Bolink, S. Graber, C. E. Housecroft, L. Sachno, M. Neuburger and E. C. Constable, *Adv. Energy Mater.*, 2011, **1**, 282–290.
43 G. E. Schneider, H. J. Bolink, E. C. Constable, C. D. Ertl, C. E. Housecroft, A. Pertegás, J. A. Zampese, A. Kanitz, F. Kessler and S. B. Meier, *Dalton Trans.*, 2014, **43**, 1961–1964.
44 S. B. Meier, W. Sarfert, J. M. Junquera-Hernández, M. Delgado, D. Tordera, E. Ortí, H. J. Bolink, F. Kessler, R. Scopelliti, M. Grätzel, M. K. Nazeeruddin and E. Baranoff, *J. Mater. Chem. C*, 2013, **1**, 58–68.
45 R. D. Costa, E. Ortí, H. J. Bolink, F. Monti, G. Accorsi and N. Armaroli, *Angew. Chem., Int. Ed.*, 2012, **51**, 8178–8211.
46 M. Y. Wong and E. Zysman-Colman, in *Light-Emitting Electrochemical Cells: Concepts, Advances and Challenges*, ed. R. D. Costa, Springer International Publishing, 2017, pp. 237–266.
47 P. Pla, J. M. Junquera-Hernández, H. J. Bolink and E. Ortí, *Dalton Trans.*, 2015, **44**, 8497–8505.

48 Q. Zhao, S. Liu, M. Shi, C. Wang, M. Yu, L. Li, F. Li, T. Yi and C. Huang, *Inorg. Chem.*, 2006, **45**, 6152–6160.
49 S.-J. Liu, Q. Zhao, Q.-L. Fan and W. Huang, *Eur. J. Inorg. Chem.*, 2008, 2177–2185.
50 Z. Li, P. Cui, C. Wang, S. Kilina and W. Sun, *J. Phys. Chem. C*, 2014, **118**, 28764–28775.
51 Y. Wu, H. Jing, Z. Dong, Q. Zhao, H. Wu and F. Li, *Inorg. Chem.*, 2011, **50**, 7412–7420.
52 J. H. Vella, A. Parthasarathy and K. S. Schanze, *J. Phys. Chem. A*, 2013, **117**, 7818–7822.
53 F. Gärtner, S. Denurra, S. Losse, A. Neubauer, A. Boddien, A. Gopinathan, A. Spannenberg, H. Junge, S. Lochbrunner, M. Blug, S. Hoch, J. Busse, S. Gladiali and M. Beller, *Chem. – Eur. J.*, 2012, **18**, 3220–3225.
54 S. T. Parker, J. D. Slinker, M. S. Lowry, M. P. Cox, S. Bernhard and G. G. Malliaras, *Chem. Mater.*, 2005, **17**, 3187–3190.